

KINEMATIC CONSTITUTIVE MODELING OF AN ALUMINUM ALLOY UNDER CYCLIC FATIGUE

Rodrigo Mendes Lima

Universidade de São Paulo – Escola de Engenharia de São Carlos
 rodrigo.mendes.lima@usp.br

Ernesto Massaroppi Junior

Universidade de São Paulo – Escola de Engenharia de São Carlos
 massarop@sc.usp.br

Abstract. *This paper proposes the application of a nonlinear kinematic model capable of predicting the behavior of an aluminum alloy (7050 T7451) under cyclic fatigue due to uniaxial loading. The model is based on the assumption that the isotropic hardening is null after the material reaches its stable hysteresis cycle, leading to a maximum Baushinger effect. The kinematic hardening is described by the model proposed by Armstrong and Frederick and modified by Chaboche. Cyclic fatigue tests were performed under controlled deformation for different strain amplitudes and with the predominance of elastic component. The experimental results obtained for each strain amplitude were simulated in ANSYS® (academic version 13.0), intending to determine and calibrate the material's constitutive parameters.*

Keywords: *cyclic fatigue, kinematic hardening, stable hysteresis cycles.*

1. INTRODUCTION

The improvements required to machine components performance lead to the adoption of new methodologies capable of predicting the material's behavior when submitted to real work conditions in order to raise the mechanical components reliability.

The necessity to understand the elastic-plastic behavior of metals comes from the fact that these materials tend to fail after a period of working time due to the damage accumulation caused by the plastic loading history.

The major part of the damage accumulation is due to the kinematic hardening, once the material's elastic domain reaches its stable condition after a few cycles. The kinematic hardening is responsible for the alterations observed in the yielding surface position and is described by the Armstrong-Frederick model.

Using data obtained from fatigue and monotonic tests, the kinematic parameters have been determined so the model could be validated using FEM simulations.

2. CONSTITUTIVE MODEL

The material's nonlinear behavior is determined by a mixed hardening model described by two parts: the isotropic hardening, which considers alterations in material's elastic domain and determines the hardening or softening behavior; and the kinematic hardening, which allows determinations about the backstress evolution. A schematic image of both the phenomena is presented as follows in Figure 1.

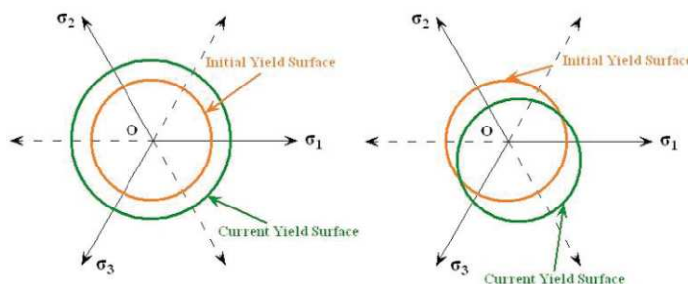


Figure 1 – Material's hardening behavior: isotropic hardening (left) and kinematic hardening (right). [5]

Both phenomena are evaluated under the Bauschinger Effect, as described in Figure 2.

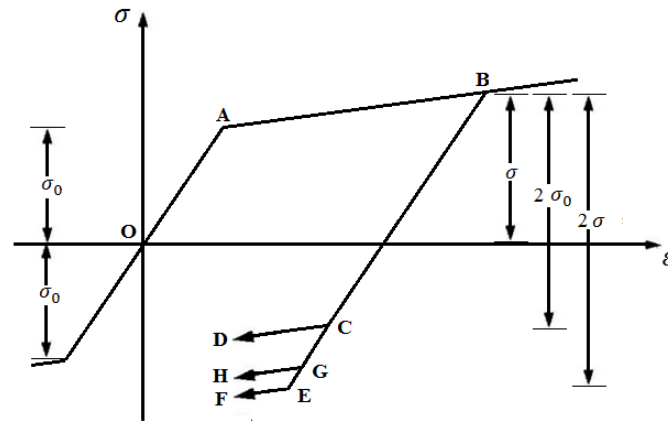


Figure 2 – Bauschinger Effect for linear hardening: kinematic hardening (pathway OABCD); isotropic hardening (pathway OABEF); and mixed hardening (pathway OABGH).[4]

Analyses of uniaxial cyclic loading indicate that the major phenomena governing the hardening behavior is the kinematic, being the isotropic portion ignored in most cases [1]. However, by allowing the elastic domain to vary, the size of the yield surface can be employed to account for transient material behavior [6]. Namely when the hysteresis cycles no longer change their configurations, it can be considered that only kinematic hardening takes place and contribute to the damage accumulation.

The mixed hardening model composition between the two phenomena is determined by the Bauschinger parameter M that separates the plastic strain into its isotropic and kinematic components, identified by the indices i and k respectively [4], as follows:

$$\varepsilon_{ij}^p = \varepsilon_{ij}^{pi} + \varepsilon_{ij}^{pk} \quad (1)$$

$$\varepsilon_{ij}^{pi} = M\varepsilon_{ij}^p \quad (2)$$

$$\varepsilon_{ij}^{pk} = (1 - M)\varepsilon_{ij}^p \quad (3)$$

$$0 \leq M \leq 1 \quad (4)$$

The Bauschinger parameter can be determined as follows [4]:

$$M = \frac{\bar{\sigma}_e - \sigma_0}{\sigma_e - \sigma_0} \quad (5)$$

The kinematic hardening rule effectiveness requires the backstress evolution to be related to the plastic strain or to the stress during the loading process [8], being the material behavior better described by its recent strain history [5]. A good solution is the utilization of a hardening rule proposed by Armstrong and Frederick and presented in Equation 9 [2], containing a recall term which incorporates the fading memory effect of the strain path and essentially makes the rule non-linear [7]. The nonlinearities are given as a recall term in the Prager's rule [3]:

$$dX_i = \frac{2}{3}C_i d\varepsilon_p - \gamma_i X_i dp \quad (6)$$

The kinematic equation describes the rapid changes due to the plastic flow during cyclic loadings and plays a role even under stabilized conditions [3].

The resulting equation for the backstress evolution in an uniaxial test is given by:

$$d\alpha_{11} = \left(\frac{c}{\sigma_0} \bar{\sigma}_{11} - \gamma \alpha_{11} \right) (1 - M) d\varepsilon_{11}^p \quad (7)$$

3. EXPERIMENTAL TESTS

The material utilized for the verification of the hardening behavior was the aluminum alloy 7050 T7451, whose composition is presented in Table 1.

Table 1 – Aluminum alloy 7050 T7451. [10]

Element	Al	Cr	Cu	Fe	Mg	Mn	Si	Ti	Zn	Zr
%	87,3 - 90,3	≤ 0,04	2 - 2,6	≤ 0,15	1,9 - 2,6	≤ 0,1	≤ 0,12	≤ 0,06	5,7 - 6,7	0,08 - 0,15

This alloy has very high strength coupled with high resistance to exfoliation corrosion and stress-corrosion cracking, high fracture toughness, and fatigue resistance. This leads to applications in aircraft structures [10].

Simple tension tests have been conducted in order to verify the material's monotonic properties. Also, fatigue tests have been realized under strain control in order to obtain the hysteresis cycles for stable conditions and strain amplitudes varying from 0,67% to 1,00%. All the experimental campaign have been realized under room temperature (25°C) at the Mechanical Properties Laboratory from EESC-USP's Materials Engineering Department, using a MTS LANDMARK servo-hydraulic machine (maximum capacity of 100kN) and strain control provided by a MTS 632.26F-20 extensometer. Figure 4 shows the specimen geometries used for the experimental campaign according to ASTM E606-04 norm.

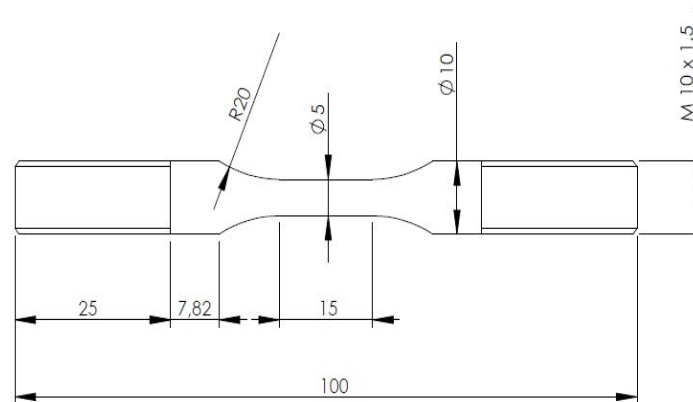


Figure 3 – Test specimen (dimensions in mm)

The results obtained from the monotonic tests are presented in Figure 5 and Table 2

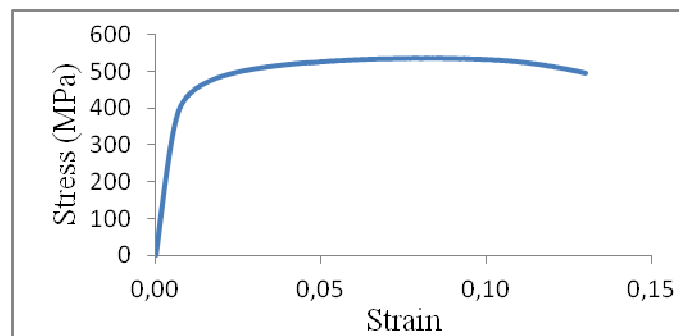


Figure 4 – Monotonic curve

Table 2 – Monotonic properties

Modulus of elasticity (GPa)	Proportional limit strength (MPa)	Ultimate strength (MPa)	Elongation at break (%)	Rupture Strength (MPa)
72	170	536	13	495

The beginning of the yield process, being a gradual transition from a linear to a non-linear stress-strain response, is difficult to be determined precisely [9]. A visual analysis has been made to find the beginning of the nonlinearities on the monotonic curves and the stable hysteresis cycles.

Rodrigo Mendes Lima, Ernesto Massaroppi Junior
Kinematic constitutive modeling of an aluminum alloy under cyclic fatigue

For the stable hysteresis cycles, the kinematic hardening has been considered as the only remaining phenomenon governing the material's behavior. During the transient life, the Bauschinger's parameter M after each loading step decreases gradually up to the point that considerable alterations on the elastic domain are no longer observed. From Equation 3:

$$\varepsilon_{11}^{pk} = \varepsilon_{11}^p \quad (8)$$

The results obtained for the stable hysteresis cycles are presented in Table 5 and Figure 6:

Table 3 – Aluminum alloy 7050 T7451 properties for the stable hysteresis cycles

ε_a	ε_{pa}	σ_a (MPa)	σ_0 (MPa)	α_{11}^{Max} (MPa)	α_{11}^{Min} (MPa)					
0,00662	0,00047	427	446	200	-207					
0,00755	0,00116	441	455	210	-217					
0,00870	0,00191	447	461	211	-222					
0,00920	0,00240	450	213	-220	0,01000	0,00295	453	473	214	-218
0,01000	0,00295	453	473	214	-218					

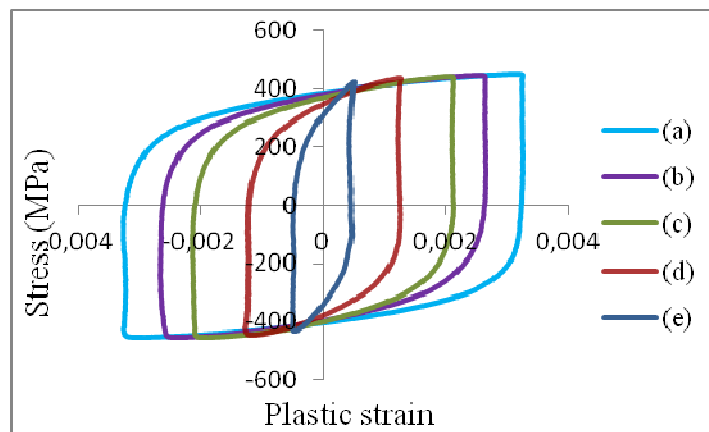


Figure 5 – Hysteresis cycles for the various strain amplitudes: 1,00% (a); 0,920% (b); 0,870% (c); 0,755% (d) and 0,662% (e).

The backstress evolution for each cycle presented in Figure 5 is shown in Figure 6:

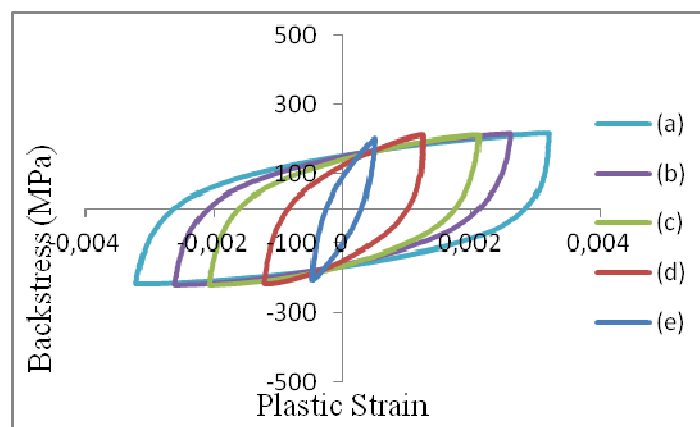


Figure 6 – Backstress curves for the various strain amplitudes: 1,00% (a); 0,920% (b); 0,870% (c); 0,755% (d) and 0,662% (e).

4. CONSTITUTIVE PARAMETERS AND FEM RESULTS

The kinematic constitutive parameters determination was made considering the Equation 12 as follows:

$$d\alpha_{11} = \left(\frac{C}{\sigma_0} \bar{\sigma}_{11} - \gamma \alpha_{11} \right) d\varepsilon_{11}^p \quad (9)$$

$$\bar{\sigma}_{11} = \sigma_{11} - \alpha_{11} = (\sigma_0 + \alpha_{11}) - \alpha_{11} \quad (10)$$

$$\frac{d\alpha_{11}}{d\varepsilon_{11}^p} = C' = (C - \gamma \alpha_{11}) \quad (11)$$

With Equation 11, it can be concluded that the parameter C' is given by the slope of the backstress curve, being C the slope observed when the plastic loading is initiated.

The determination of γ was realized over the translated portion of the tensile backstress curves (Figure 7), considering the compression portion symmetrical to it. The curves were approximated by power functions of the form:

$$\alpha_d = A\varepsilon_{pd}^B \quad (12)$$

$$\alpha_d = \alpha_{11} - \alpha_{11}^{Min} \quad (13)$$

$$\varepsilon_{pd} = \varepsilon_{11}^p - \varepsilon_{11}^{p Min} \quad (14)$$

Being $\varepsilon_{11}^{p Min}$ the slowest ε_{11}^p in the backstress curves.

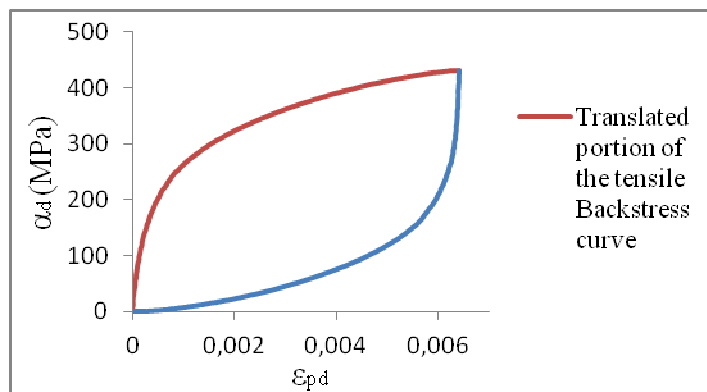


Figura 7 – Translated backstress curve for the strain amplitude equal to 1,00%.

Considering the differentiation of a generic function $ax - e^{f(x)} + R$ (being R a constant) in terms of x , it can be found that:

$$\frac{d(ax - e^{f(x)})}{dx} = a - f'(x)e^{f(x)} \quad (15)$$

From Equations 11 and 15:

$$\alpha_d = C\varepsilon_{pd} - e^{f(\varepsilon_{pd})} + e^{f(0)} \quad (16)$$

$$C' = \frac{d\alpha_d}{d\varepsilon_{pd}} = C - f'(\varepsilon_{pd})e^{f(\varepsilon_{pd})} = C - \gamma\alpha_d \quad (17)$$

$$\gamma = \frac{f'(\varepsilon_{pd})e^{f(\varepsilon_{pd})}}{\alpha_d} \quad (18)$$

Considering the power function presented in Equation 12:

$$f(\varepsilon_{pd}) = \ln(C\varepsilon_{pd} - A\varepsilon_{pd}^B) \quad (19)$$

Rodrigo Mendes Lima, Ernesto Massaroppi Junior
Kinematic constitutive modeling of an aluminum alloy under cyclic fatigue

$$f'(\varepsilon_{pd}) = \frac{C-AB\varepsilon_{pd}^{B-1}}{C\varepsilon_{pd}-A\varepsilon_{pd}^B} \quad (20)$$

$$\gamma = \left(\frac{1}{A\varepsilon_{pd}^B} \right) \frac{C-AB\varepsilon_{pd}^{B-1}}{C\varepsilon_{pd}-A\varepsilon_{pd}^B} e^{\ln(C\varepsilon_{pd}-A\varepsilon_{pd}^B)} = \frac{C-AB\varepsilon_{pd}^{B-1}}{A\varepsilon_{pd}^B} \quad (21)$$

Intending to avoid infinite values of C as predicted by the power functions, it was chosen finite ones in agreement with the backstress curves. Similarly, the initial value of γ (γ_0) was determined as the highest one corresponding to the defined C and $\varepsilon_{pd0} = (C/A)^{1/(B-1)}$, being $\varepsilon_{pd} = \varepsilon_{pd0} > 0$. For $0 < \varepsilon_{pd} < \varepsilon_{pd0}$, γ was not defined, being $C' = C$. The values of A , B , C and γ_0 obtained for each strain amplitude are presented in Table 4.

Table 4 – Power functions coefficients and γ_0 for each strain amplitude.

ε_a	A (MPa)	B	C (GPa)	γ_0
0,00662	8080	0,444	11790	209000
0,00755	3729	0,360	11670	168000
0,00870	2433	0,311	11600	143000
0,00920	2032	0,290	11570	135000
0,01000	1718	0,274	11560	133000

Figure 8 shows the evolution of the data presented in Table 4 as a plastic strain amplitude function.

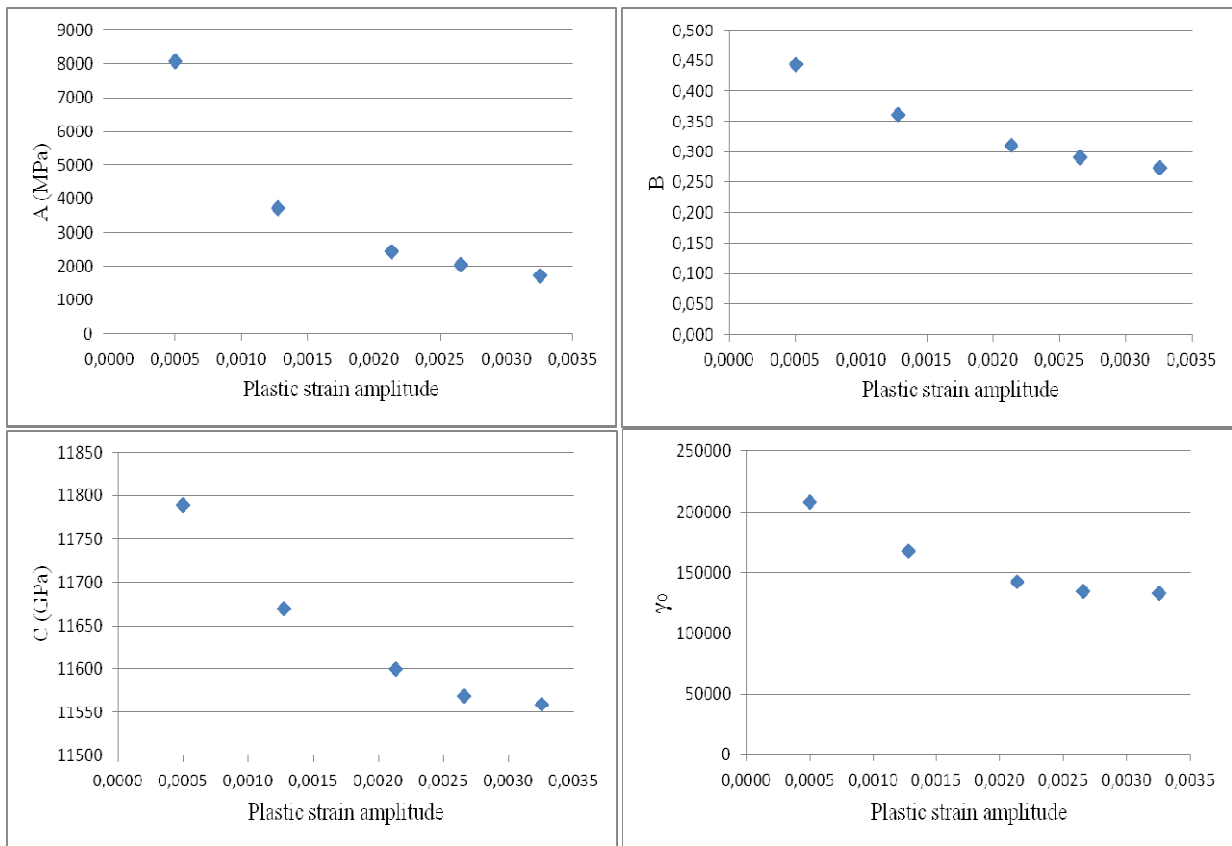


Figura 8 – Evolution of A , B , C and γ_0 in terms of the plastic strain amplitude.

Figure 9 shows the evolution of γ as a plastic strain function for each strain amplitude.

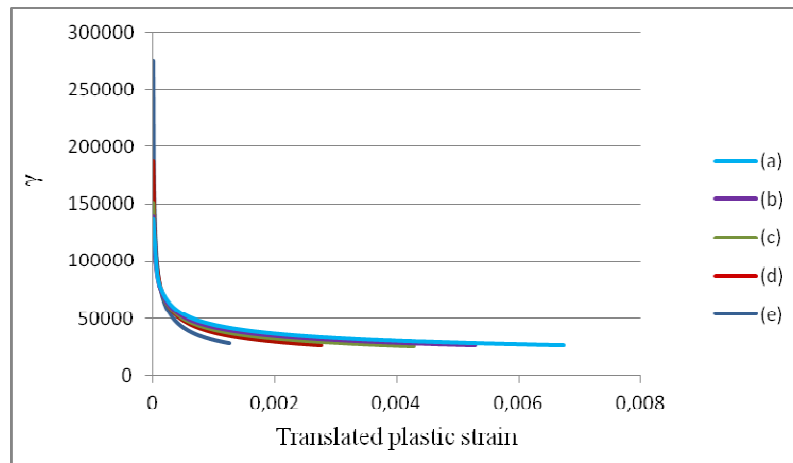


Figure 9 – Evolution of γ as a plastic strain function for the various strain amplitudes: 1,00% (a); 0,920% (b); 0,870% (c); 0,755% (d) and 0,662% (e).

A code containing the kinematic nonlinear model was implemented in ANSYS 13 (Mechanical APDL version) over discrete plastic strain intervals along the kinematic curves in order to consider the evolution of γ over the entire plastic strain domain for fixed values of C .

The simplicity of the analysis section geometry allowed the utilization of a single element in the FEM model, constituted by 8 nodes, each one containing 3 degrees of freedom related to the translation over the coordinate axes. A comparison between the results for a refined mesh and a single element model has shown no significant discrepancies.

The results are presented in Figure 10 for the stable cycles.

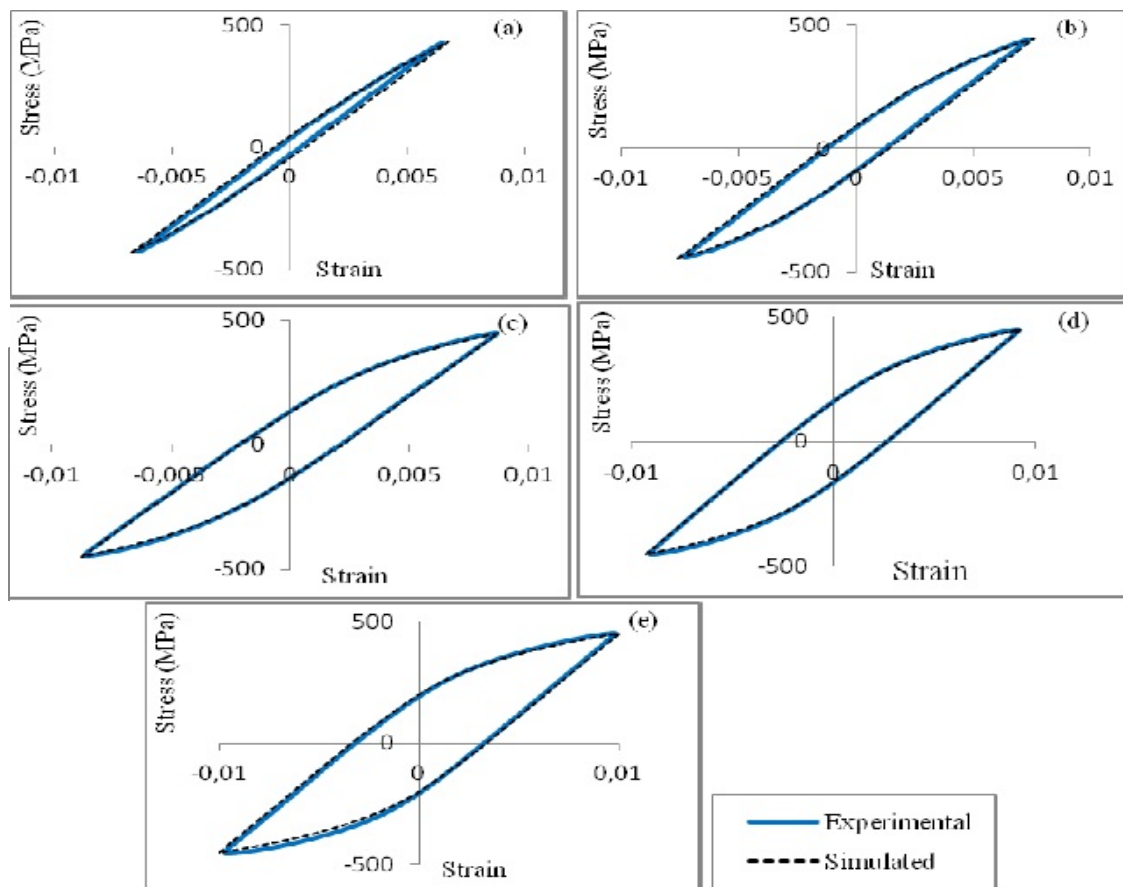


Figure 10 – Stable hysteresis cycles for different strain amplitudes: 0,662 (a); 0,755% (b); 0,870% (c); 0,920% (d) and 1,000% (e).

Rodrigo Mendes Lima, Ernesto Massaroppi Junior
Kinematic constitutive modeling of an aluminum alloy under cyclic fatigue

Figure 10 shows the discrepancies are minimal.

5. RESULTS DISCUSSION

It can be seen in Figure X that the power functions coefficients and the values of the kinematic hardening model (C and γ_0) tends to a stable configuration when the plastic strain amplitude is increased. The same can be noted for the γ evolutionary behavior in terms of the translated plastic strain (ε_{pd}), shown in Figure F.

The fact that only kinematic hardening takes place in the stable hysteresis cycles indicates that M has a smoother evolution for each loading step, being null when alterations in the elastic domain are no longer observed.

The smaller the plastic strain amplitude the higher the values of C and γ_0 . This fact explains why the curves with small strain amplitude have higher initial slopes, tending to stable configurations faster at the loading very beginning, as can be seen in Figure 6, once γ controls the backstress stabilization velocity.

It is remarkable that the presented methodology accuracy depends on how good the power functions describe the real backstress curves.

6. CONCLUSIONS

The presented work has provided a good way to describe the aluminum alloy 7050 T7451 submitted to cyclic loadings. The results accuracy depended on how good the power functions described the real backstress evolution as plastic loading occurred, allowing the study of each kinematic parameter and power function coefficient evolution in terms of both the plastic strain amplitude and the translated plastic strain. Once the behavior pattern indicates the coefficients A , B and the parameters C and γ_0 , just as γ , will stabilize, the hysteresis cycles can be foreseen for this material when submitted to higher strain amplitudes.

The models implemented in the FEM commercial code have provided good results compared to those obtained in the fatigue tests, once the parameters have been considered as variables instead of the constants foreseen in the the Armstrong-Frederick kinematic model.

Comparisons between the elastic domain for the material free of plastic loading history and those observed at the stable cycles indicate the material obeys the Drucker's stability criteria.

The isotropic hardening is observed during the material's transient life, which corresponds to the first ten cycles, approximately. After this, the only phenomenon that remains and contributes to the damage accumulation is the kinematic hardening. This gives precedent for the development of damage accumulation laws based only on the backstress evolution.

7. NOMENCLATURE

ε_{ij}^p – Plastic strain tensor
 ε_a – Strain amplitude
 ε_{pa} – Plastic strain amplitude
 ε_{pd} – Translated plastic strain
 p, ε_p – Equivalent plastic strain
 M – Bauschinger Parameter
 $\bar{\sigma}_{ij}$ – Reduced stress tensor
 $\bar{\sigma}_e$ – Equivalent Stress
 σ_a – Stress amplitude
 σ_0 – Half of the elastic domain
 X_i, α_{ij} – Backstress tensor
 α_d – Translated backstress
 R_∞, R_0, b – Isotropic constitutive parameters
 C, γ – Kinematic constitutive parameters

8. ACKNOWLEDGMENTS

The researches involved in this article have received support from CAPES. This is gratefully acknowledged.

9. REFERENCES

- [1] ABDEL-KARIM, M., **Shakedown of complex structures according to various hardening rules**, Int J Pres Ves Pip 2005;82(6):427–58.
 [2] ARMSTRONG, P. J.; FREDERICK, C.O., **A Mathematical Representation of the Multiaxial Bauschinger Effect**, G.E.G.B. Report RD/B/N 731, 1966.

22nd International Congress of Mechanical Engineering (COBEM 2013)
November 3-7, 2013, Ribeirão Preto, SP, Brazil

- [3] CHABOCHE, J. L., **CONSTITUTIVE EQUATIONS FOR CYCLIC PLASTICITY AND CYCLIC VISCOPLASTICITY**, International Journal of Plasticity, v.5, pp. 247-302, 1989
- [4] CHEN, W-F., **Constitutive Equations for Engineering Materials - Volume 2: Plasticity and Modeling**, Amsterdam: Elsevier, 1994
- [5] GUO, J.; XIN, K.; HE, M. **Comparative study and application of a coupled nonlinear kinematic hardening model for structural metallic material behavior**, Procedia Engineering, v.10, pp. 262-269, 2011
- [6] JIANG, Y.; KURATH, P., **CHARACTERISTICS OF THE ARMSTRONG-FREDERICK TYPE PLASTICITY MODELS**, International Journal of Plasticity, Vol. 12, No. 3, pp. 387-415, 1996
- [7] MAHBADI, H.; ESLAMI, M. R., **Cyclic loading of beams based on the Prager and Frederick – Armstrong kinematic hardening models**, International Journal of Mechanical Sciences, v.44, pp. 859 – 879, 2002
- [8] SKRZYPEK, J. J.; HETNARSKI, R. B., **PLASTICITY and CREEP: Theory, Examples and Problems**, Boca Raton: CRC Press, 2000
- [9] VALANIS, K.C., **A Theory of Viscoplasticity without a Yield Surface**, Part I. Application to Mechanical Behavior of Metals," Arch. Mech., 23, 535, 1971
- [10] MatWeb – Material Property Data, Aluminum 7050-T7451 (7050-T73651) [Accessed in February 2, 2012]. Available in <www.matweb.com>.

10. RESPONSIBILITY NOTICE

The authors are the only responsible for the printed material included in this paper.